Hindawi
Mathematical Problems in Engineering
Volume 2019, Article ID 6190159, 15 pages
https://doi.org/10.1155/2019/6190159

Research Article

Seismic Fragility Analysis of Steel Liquid Storage Tanks Using Earthquake Ground Motions Recorded in Korea

Sangmok Lee, Byungmin Kim, and Young-Joo Lee

School of Urban and Environmental Engineering, Ulsan National Institute of Science and Technology (UNIST), Ulsan 44919, Republic of Korea

Correspondence should be addressed to Young-Joo Lee; ylee@unist.ac.kr

Received 9 April 2019; Revised 22 June 2019; Accepted 27 June 2019; Published 15 July 2019

Academic Editor: Francisco J. Montáns

Liquid-containing storage tanks are important structures in industrial complexes. Because earthquake damages to liquid storage tanks can cause structural collapse, fires, and hazardous material leaks, there have been continuous efforts to mitigate earthquake damages using seismic fragility analysis. In this regard, this study focuses on the seismic responses and fragility of liquid storage tanks. First, the characteristics of earthquake ground motions are a critical factor influencing the seismic fragility of structures; thus, this study employs real earthquake records observed in the target area, southeastern Korea, with the earthquake characteristics estimated based on the ratio of peak ground acceleration to peak ground velocity. When a liquid storage tank oscillates during an earthquake, additional forces can impact the tank wall owing to hydrodynamic pressures. Therefore, this study presents a sophisticated finite element (FE) model that reflects the hydrodynamic effect of an oscillating liquid. Another advantage of such an FE model is that detailed structural responses of the entire wall shells can be estimated; this is not possible in simplified lumped mass or surrogate models. Lastly, probabilistic seismic demand models are derived for three critical limit states: elastic buckling, elephant's foot buckling, and steel yielding. Using the real earthquake ground motion records, constructed FE model, and limit states, a seismic fragility analysis is performed for a typical anchored steel liquid storage tank in Korea. In addition, for comparison purposes, a ring-stiffened model is investigated to derive a seismic fragility curve. The results of the seismic fragility assessment show that elastic buckling is the most vulnerable damage state. In contrast, elephant's foot buckling and steel yielding indicate relatively severe damage levels. Furthermore, it is observed that ring stiffeners decrease the elastic buckling damage, although there is no practical effect on elephant's foot buckling and steel yielding in all ground motion intensities.

1. Introduction

Liquid storage tanks are a major component of industrial complexes. When a storage tank containing liquid is subjected to seismic loads, it can be damaged and collapsed, potentially causing the leakage of hazardous materials and major fires. According to Persson and Lönnermark [1], the 1964 Niigata earthquake in Japan led to fires that resulted in the loss of 97 tanks containing 1.1 million barrels of crude. It was also reported that 29 tanks were damaged or leaked owing to the impact of the 2003 Hokkaido earthquake. In Turkey, three naphtha tanks and a crude oil tower were damaged owing to the 1999 İzmit earthquake.

According to statistical data obtained from the Korea Industrial Complex Corporation [2], there are 1189 industrial complexes in Korea; in particular, there are 436 industrial complexes in southeastern Korea, as of 2018. In addition, earthquakes have frequently occurred in the southeastern part of Korea in recent years, exposing these many industrial complexes to seismic hazards. Thus, the importance of structural risk assessment has become increasingly important, and there have been continuous efforts to mitigate earthquake damages using seismic fragility analyses [3, 4]. This study concentrates on the structural fragility of liquid storage tanks.

The characteristics of earthquake ground motions are also a critical factor in the seismic fragility of structures. Previous studies [3–6] investigated the seismic fragility of structures with various types of earthquake ground motions to determine the effects of ground motion characteristics.

The analysis results of these studies showed that earthquake damages to structures varied with different ground motion properties. In addition, for an accurate seismic fragility analysis of structures, numerous studies on seismic fragility assessments using analytical models [3–10] have utilized real ground motion records from world-wide well-known earthquakes. However, these records may not reflect the characteristics of a specific region. In this study, real ground motion records observed in the target area (i.e., southeastern Korea) are intensively collected and used in seismic fragility estimation for a more realistic simulation.

When a steel liquid storage tank is exposed to an earthquake, additional forces can impact the tank wall owing to hydrodynamic pressures. The hydrodynamic response of the liquid in a tank can be described by two distinct modes: convective and impulsive [11]. The upper part of the liquid, having convective motion (often called the sloshing), exhibits a long period oscillation, whereas the lower part of the liquid moves together with the tank wall as though rigidly attached to the tank. Veletsos [12] investigated the seismic effects of a flexible liquid storage tank and found that hydrodynamic forces could have a greater influence on a flexible tank than on a rigid one.

Dynamic buckling mainly appears in an oscillating liquid-filled tank owing to the liquid-tank interaction, and many researchers have explored the buckling of steel tanks subjected to seismic loads with numerical models [9, 13–15]. These studies have demonstrated the need for a sophisticated model of structural analysis that can account for hydrodynamic pressures when analyzing the seismic response and fragility of a liquid storage tank.

Seismic fragility analyses for liquid storage tanks have been performed in recent years. Buratti and Tavano [9] derived seismic fragility curves for the buckling of the tank wall using an added-mass approximate model for liquid modeling. Paolacci et al. [16] concentrated on the seismic fragility of a liquid storage tank in terms of the buckling of the tank wall with simplified numerical models. Phan et al. [10] used lumped mass models and considered the buckling failure of the tank wall for seismic fragility assessment. However, the aforementioned studies considered the liquid-tank interaction using simplified tank models in their seismic fragility analyses. Lee et al. [6] developed an advanced FE model to take into account hydrodynamic pressures, but the buckling failure was not considered. In addition, these studies utilized worldwide well-known earthquake records in their fragility assessment.

In this study, the seismic risk of a typical anchored cylindrical storage tank is investigated, and seismic fragility curves are derived. Real ground motion data reflecting the characteristics of the target region are collected and used. To consider hydrodynamic effect, a sophisticated FE model is constructed by referring to an example model used in a previous study [17]. Using the FE model, the structural responses are analyzed by nonlinear time-history analyses. The elastic buckling, elephant's foot buckling, and steel yielding of the tank wall are introduced as critical limit states of the tank for the fragility analysis.

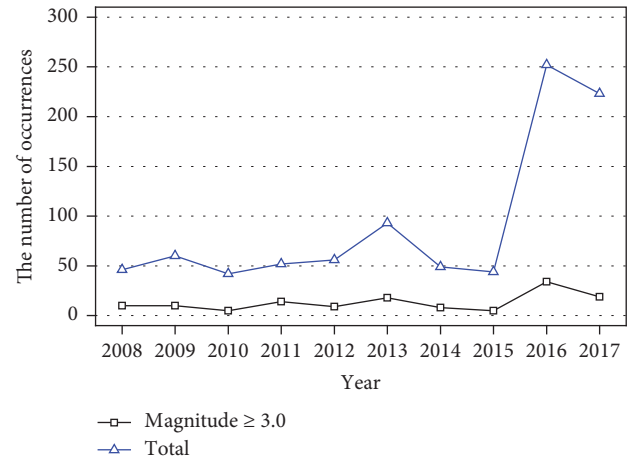

Figure 1: Earthquake occurrence trend in Korea.

2. Earthquake Ground Motions

In recent years, earthquake occurrences have increased in the Korean Peninsula. Figure 1 presents the number of earthquake occurrences from 2008 to 2017 in Korea. As shown in the figure, the number of earthquake occurrences increased significantly in 2016 and 2017, and the earthquake events (≥ local magnitude, M_L3.0) were also prevalent in this period.

Table 7 summarizes 52 earthquakes records (≥ M_L3.0) that occurred in southeastern Korea from 2008 to 2017, observed in the Ulsan Seismological Observatory. These records were obtained from the National Earthquake Comprehensive Information System (NECIS) database [19], which is operated by the Korea Meteorological Administration (KMA). Among these 52 earthquakes, the strongest one was the 12 September 2016 M_L5.8 Gyeongju earthquake and the second strongest one was the 15 November 2017 M_L5.4 Pohang earthquake, both of which triggered numerous aftershocks.

2.1. Characteristics of Earthquake Ground Motions. Characteristics of earthquake ground motions are highly dependent on various factors, including earthquake magnitudes, fault types, soil conditions, and source-to-site distances [20]. Particularly, it is well known that Korea is situated in the seismically stable region [21] and soil and rock conditions are different from other regions [22], resulting in unique earthquake ground motion characteristics in Korea. Hence, it is necessary to ascertain the characteristics of earthquake ground motions in the area under consideration prior to the assessment of a structure's seismic fragility. The ratio of the peak ground acceleration (PGA) to the peak ground velocity (PGV), which is commonly called the a/v ratio, is an informative measure for understanding the characteristics of earthquake ground motions [23–25]. The a/v ratios are typically classified as low, intermediate, and high. Previous studies [3–6] have developed seismic fragility curves of structures with different a/v ratios and emphasized the importance of the characteristics of earthquake ground motions on the seismic fragility. This is related to the relationship of

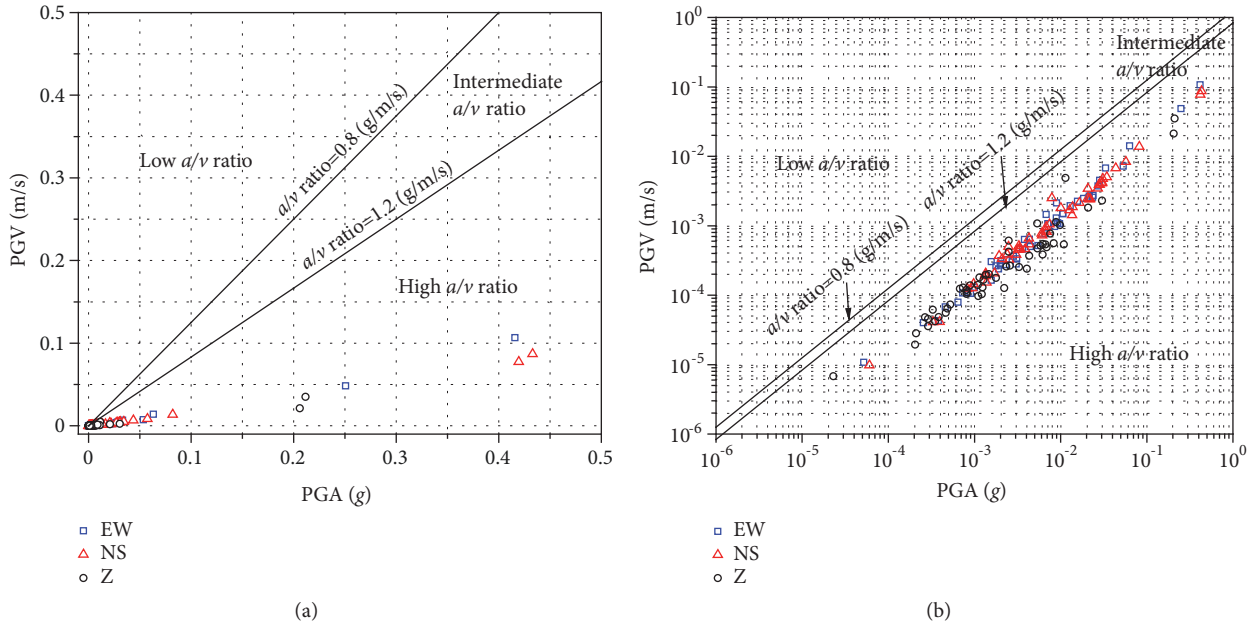

Figure 2: Classification of the 52 earthquake ground motions based on the a/v ratios: (a) in the arithmetic scale and (b) in the common logarithm (base 10) scale.

the earthquake magnitudes with the epicentral distances, frequency properties, and durations of ground motions. For example, earthquake ground motions included in the high a/v category mostly are associated with relatively low- to moderate-magnitude earthquakes and have high frequency components and short durations, compared to those in the low a/v category [23–25].

In this study, the 52 earthquake accelerograms (Table 7) are analyzed. The gain factor is used to convert a binary expression (i.e., count) for the voltage intensity into acceleration units [26]. The gain factor varies with the types of accelerographs and data-loggers; the values used here are 2.15×10^6 count/m/s^2 (before August 2016) and 1.71×10^6 count/m/s^2 (after August 2016). This study applied the time-domain recursive filter [27] to the raw acceleration time series. The accelerograms are recorded in three directions: two horizontal components, east-west (EW) and north-south (NS), and one vertical component (Z). For each direction, the PGA and PGV values are estimated. The 52 earthquake ground motions are then categorized by the a/v ratios as low ($a/v < 0.8$ g/m/s), intermediate (0.8 g/m/s $\leq a/v \leq$ 1.2 g/m/s), and high (1.2 g/m/s $< a/v$). The three ranges of a/v ratios correspond to the three zonal combinations (i.e., $Z_a < Z_v$, $Z_a = Z_v$, and $Z_a > Z_v$) in National Building Code of Canada (NBCC) (NRCC, 1985) [28]. Z_a and Z_v denote the acceleration-related and velocity-related seismic zones, respectively. These seismic zones are based on results from statistical analyses of past earthquakes in Canada [29]. Figure 2 shows the results of the a/v classification. In the figure, the left graph presents the results in the arithmetic scale, and a graph of the common logarithm scale (base 10) is plotted on the right to show the distribution of the results more clearly. It is found in the figure that all of the ground motions are included in the high a/v level, indicating that the earthquake ground motions that occurred in southeastern Korea have high-frequency and short-duration motion features, as explained above. Thus, it is important to derive seismic fragility curves based on real earthquake ground records which can present such ground characteristics.

2.2. Input Ground Motions for Seismic Fragility Analysis. Practical seismic design guidelines, such as ASCE 7-05 [30], Eurocode 8-1 [31], and FEMA 368 [32], recommend a proper number of input ground motions. The provisions of seismic design codes were summarized in a review paper by Beyer and Bommer [33], suggesting the use of at least seven records for the seismic analysis and design of a structure. Thus, for a seismic fragility analysis, this study uses seven accelerogram data out of the 52 earthquake accelerograms for nonlinear time-history analyses. Using seven real earthquake ground motions not only enables reflection of the dynamic properties (i.e., high a/v ratio) of the region, but also considers the uncertainty of input ground motions.

Among the earthquake events presented in Table 7, the seven earthquakes with the largest magnitudes are selected for the nonlinear time-history analyses: M_L5.8, M_L5.4, M_L5.1, M_L5.0, M_L4.5, M_L4.3, and M_L4.0. Figure 13 shows the ground acceleration time-histories adopted in the analyses. Both the horizontal components (EW and NS) of each earthquake ground motion were simultaneously assigned to the structure.

3. FE Model of Steel Liquid Storage Tank

This study aims to derive the seismic fragility of a steel tank containing liquids, which is an important facility of industrial

Table 1: Material properties of the FE model.

Material	Density (kg/m^3)	Young's modulus (GPa)	Poisson's ratio
Steel	7850	203.395	0.3
Liquid (Gasoline)	680	-	-

Table 2: Earthquake events (Di Carluccio et al. [17] and European Strong-Motion Database [34]).

Code	Earthquake event	Date	Country	Station name	PGA (g)
000196xa	Montenegro	04/15/1979	Yugoslavia	Petrovac-Hotel Olivia	0.45
006334xa	South Iceland (aftershock)	06/21/2000	Iceland	Solheimar	0.42
000199ya	Montenegro	04/15/1979	Yugoslavia	Bar-Skupstina Opstine	0.36
000535ya	Erzincan	03/13/1992	Turkey	Erzincan-Meteorologij Mundurlugu	0.51
006263ya	South Iceland	06/17/2000	Iceland	Kaldarholt	0.51
006328ya	South Iceland (aftershock)	06/21/2000	Iceland	Kaldarholt	0.39
006334ya	South Iceland (aftershock)	06/21/2000	Iceland	Solheimar	0.72

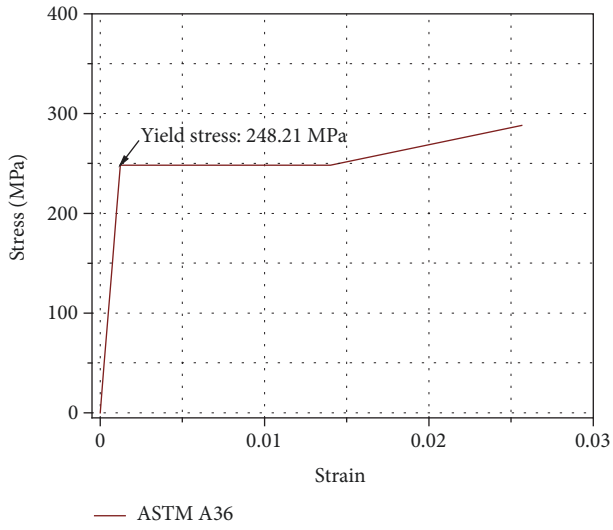

Figure 3: Material nonlinearity of ASTM A36 [18].

complexes, considering the hydrodynamic forces caused by oscillating liquids. Steel tanks can be classified to two groups, anchored and unanchored tanks, and it has been reported that their dynamic behaviors are quite different [35, 36]. This study examines the seismic fragility of an anchored steel liquid storage tank, which was relatively less well studied in previous studies but still an important facility of industrial complexes. In addition, two tank models, with and without ring stiffeners, are investigated for comparison purposes.

An FE model is constructed using a commercial FE software package, ABAQUS. The steel tank considered here is a typical steel tank and was introduced as a numerical example in a previous study [17]. It is assumed that the steel tank is made of ASTM A36 [18], whose material nonlinearity is presented in Figure 3, and the steel tank contains liquid (gasoline). Table 1 presents the material properties of the steel and liquid. The steel and liquid are modeled using shell elements (S4) and continuum elements (C3D8), respectively. To account for hydrodynamic effects in an oscillating tank, a dynamic viscosity (0.006 Pa·s) and linear U_s (shock velocity) $-U_p$ (particle velocity) Hugoniot form of the Mie-Grüneisen equation of state with a velocity of sound of 1250 m/s in liquid are applied. Grüneisen's gamma (Γ_0) and the linear Hugoniot slope coefficient (s) are assumed to be zero.

For comparison purposes, a ring-stiffened FE model is also constructed. In general, ring stiffeners are employed to improve resistance to buckling, and this study aimed to quantify the increase of the tank's buckling resistance against seismic loads. The ring-stiffened model has the same shape and material properties as the unstiffened model, and two ring stiffeners are added at the top and middle of the tank wall. Both stiffeners have the same cross-sections and dimensions. The dimensions of the ring stiffeners are properly designed by referring to the API 650 design code [37] and Sun et al. [38]. Figure 4 presents the geometric details of the liquid storage tank and ring stiffener, and Figure 5 shows the FE models in ABAQUS with and without ring stiffeners.

To validate the constructed FE model, its seismic responses in terms of peak sloshing liquid height are compared with those of a previous study [17], in which seven representative earthquake ground motions were used. Table 2 provides the details of the seven earthquakes. Nonlinear time-history analyses are performed using the seven ground motions and the constructed ABAQUS FE model. Figure 6 shows a comparison with the analysis results with those of Di Carluccio et al. [17]. The maximum estimated difference is 0.50 m (i.e., 4.19%), which is within an allowable range.

4. Seismic Fragility Assessment

In a fragility curve, the failure probability (P_f) generally defines the conditional probability of the seismic demand (D) and exceeding capacity (C) given an intensity measure (IM), as in (1) [39]. Thus, as stated by Phan and Paolacci and Bakalis et al. [10, 40], it is important to select IM in seismic fragility assessment. This study aims to derive the seismic fragility curves of liquid storage tanks using real earthquake ground motions that can reflect the characteristics. In previous

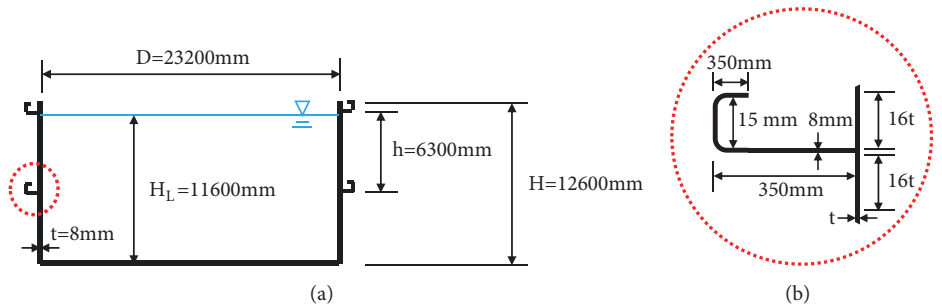

Figure 4: Geometry of the ring-stiffened model: dimensions of the (a) liquid storage tank and (b) ring stiffener.

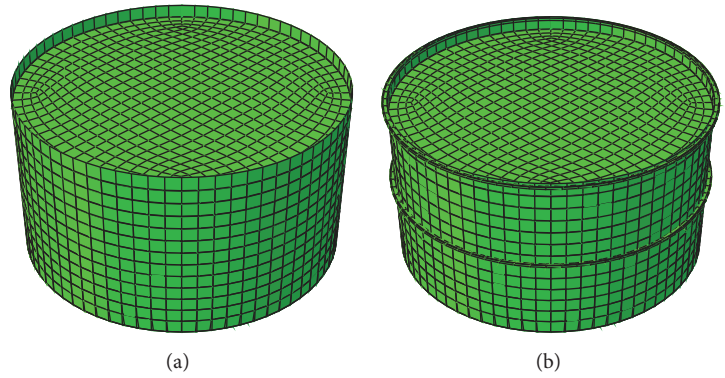

Figure 5: FE models in ABAQUS: (a) unstiffened and (b) ring-stiffened models.

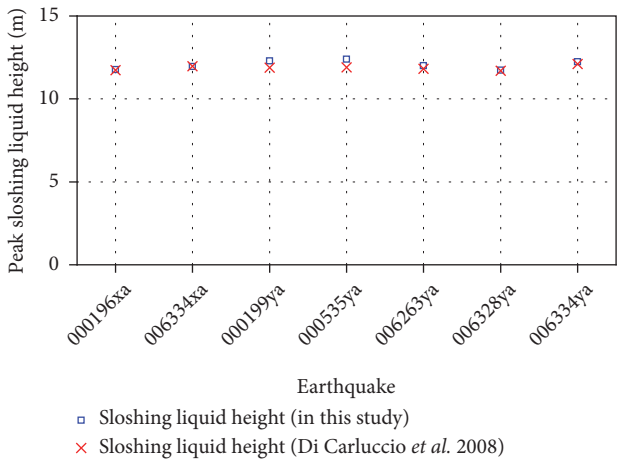

Figure 6: Peak sloshing liquid height validation.

studies [3, 4], the characteristics of collected ground motions were analyzed based on PGA/PGV (a/v) ratios, and PGA is selected as IM in this study.

$$P_f = \mathrm{P}\left[D \geq C \mid IM\right] \tag{1}$$

As the first step to calculate a failure probability, nonlinear time-history analyses are performed with varying IM values. Based on the results, probabilistic seismic demand models (PSDMs) are constructed by linear regression of the seismic responses and corresponding IM values [41]. The PSDMs have been broadly utilized to derive the analytical seismic fragility curves of various structures [7, 10, 16, 39, 42–46].

For the linear regression, it is assumed that the seismic demand (D) is expressed by the following approximation [47]:

$$D = k \bullet IM^p \tag{2}$$

where k and p are the parameters that are determined from the linear regression. By taking the natural logarithms of both sides of (2), the following linear equation is obtained:

$$\ln\left(D\right) = \ln\left(k\right) + p \cdot \ln\left(IM\right) \tag{3}$$

Using (3) and the results of the nonlinear time-history analyses with varying IM values, the unknown parameters (k and p) can be determined by a linear regression analysis. The logarithmic dispersion of the demand given IM, $\beta_{D|IM}$, can be

Table 3: Original and scaled PGA values for the primary and secondary components of the input ground motions.

No.	Magnitude	Component	Original PGA (g)	Scaled PGA (g)						
1	5.8	NS	0.4329	0.1	0.2	0.3	0.4	0.5	0.6	0.7
		EW	0.4159	0.0961	0.1921	0.2882	0.3843	0.4804	0.5764	0.6725
2	5.4	EW	0.0333	0.1	0.2	0.3	0.4	0.5	0.6	0.7
		NS	0.0309	0.0928	0.1856	0.2784	0.3712	0.4640	0.5568	0.6495
3	5.1	NS	0.4196	0.1	0.2	0.3	0.4	0.5	0.6	0.7
		EW	0.2506	0.0597	0.1194	0.1792	0.2389	0.2986	0.3583	0.4181
4	5.0	EW	0.0090	0.1	0.2	0.3	0.4	0.5	0.6	0.7
		NS	0.0079	0.0878	0.1756	0.2633	0.3511	0.4389	0.5267	0.6144
5	4.5	NS	0.0822	0.1	0.2	0.3	0.4	0.5	0.6	0.7
		EW	0.0633	0.0770	0.1540	0.2310	0.3080	0.3850	0.4620	0.5391
6	4.3	NS	0.0074	0.1	0.2	0.3	0.4	0.5	0.6	0.7
		EW	0.0068	0.0919	0.1838	0.2757	0.3676	0.4595	0.5514	0.6432
7	4.0	NS	0.0032	0.1	0.2	0.3	0.4	0.5	0.6	0.7
		EW	0.0019	0.0594	0.1188	0.1781	0.2375	0.2969	0.3563	0.4156

Table 4: Coefficients of the PSDMs.

Model type	Limit state	k	p
Unstiffened tank	Elastic buckling	0.0260	0.3335
	Elephant's foot buckling	35.5397	0.1723
	Steel yielding	269.2661	0.2402
Ring-stiffened tank	Elastic buckling	0.0155	0.2942
	Elephant's foot buckling	38.4978	0.3810
	Steel yielding	268.2180	0.2307

calculated by (Nielson and DesRoches [42] and Mangalathu et al. [43]):

$$\beta_{D|IM} \cong \sqrt{\frac{\sum_{i=1}^{N} \left(\ln\left(d_i - \ln\left(D\right)\right)\right)^2}{N-2}} \tag{4}$$

where d_i is the peak demand value obtained from the nonlinear time-history analyses and N is the total number of ground motions.

Assuming lognormal distributions for both the demand and capacity, the failure probability P_f in (1) is specifically expressed as follows:

$$P_f = \mathrm{P}\left[\mathrm{D} \geq \mathrm{C} \mid IM\right] = \Phi\left(\frac{\ln\left(S_D\right) - \ln\left(S_C\right)}{\sqrt{\beta_{D|IM}^2 + \beta_C^2}}\right) \tag{5}$$

where S_D and S_C are the median values of the demand and capacity, respectively; β_C is the logarithmic dispersion of the capacity given IM; and $\Phi(\cdot)$ is the standard normal cumulative distribution function.

4.1. Nonlinear Time-History Analyses. Using each of the input ground motions, nonlinear time-history analyses are performed with varying earthquake intensities. This parametric analysis method is known as an incremental dynamic analysis (IDA) [48]. Both horizontal components of each input ground motion are applied simultaneously. The input ground motions are scaled in such a way that the component with the higher PGA (primary) becomes the designated value, and the other component (secondary) is then also adjusted by the same scaling factor [49]. Table 3 summarizes the original and scaled PGA values for the primary and secondary components of the input ground motions.

As a result, the PSDMs are derived for each of the selected limit states (i.e., elastic buckling, elephant's foot buckling, and steel yielding) using (3). Each damage state is analyzed in terms of radial displacement, compressive meridional stress, and von-Mises stress, respectively. Figure 7 shows the PSDMs of the unstiffened model using a log-log scale. Table 4 presents the regression coefficients of the PSDMs (i.e., k and p in (3)).

As mentioned above, dynamic buckling is a well-known structural behavior of steel liquid storage tanks subjected to earthquake ground motions. Buratti and Tavano [9], Virella et al. [13], Djermane et al. [14], and Sobhan et al. [15] investigated the buckling stability of steel tanks with numerical models. The buckling phenomena in a liquid-oscillating steel tank are generally classified as elastic and elastoplastic buckling. The former includes diamond-shaped buckling and secondary buckling, while the latter is often called elephant's foot buckling [9, 13]. This study deals with both elastic and elephant's foot buckling phenomena. The former is typically found at the upper part of the steel tank, which has a larger deflection than the lower part, and the latter commonly exhibits a bulge of the near the bottom of the tank wall.

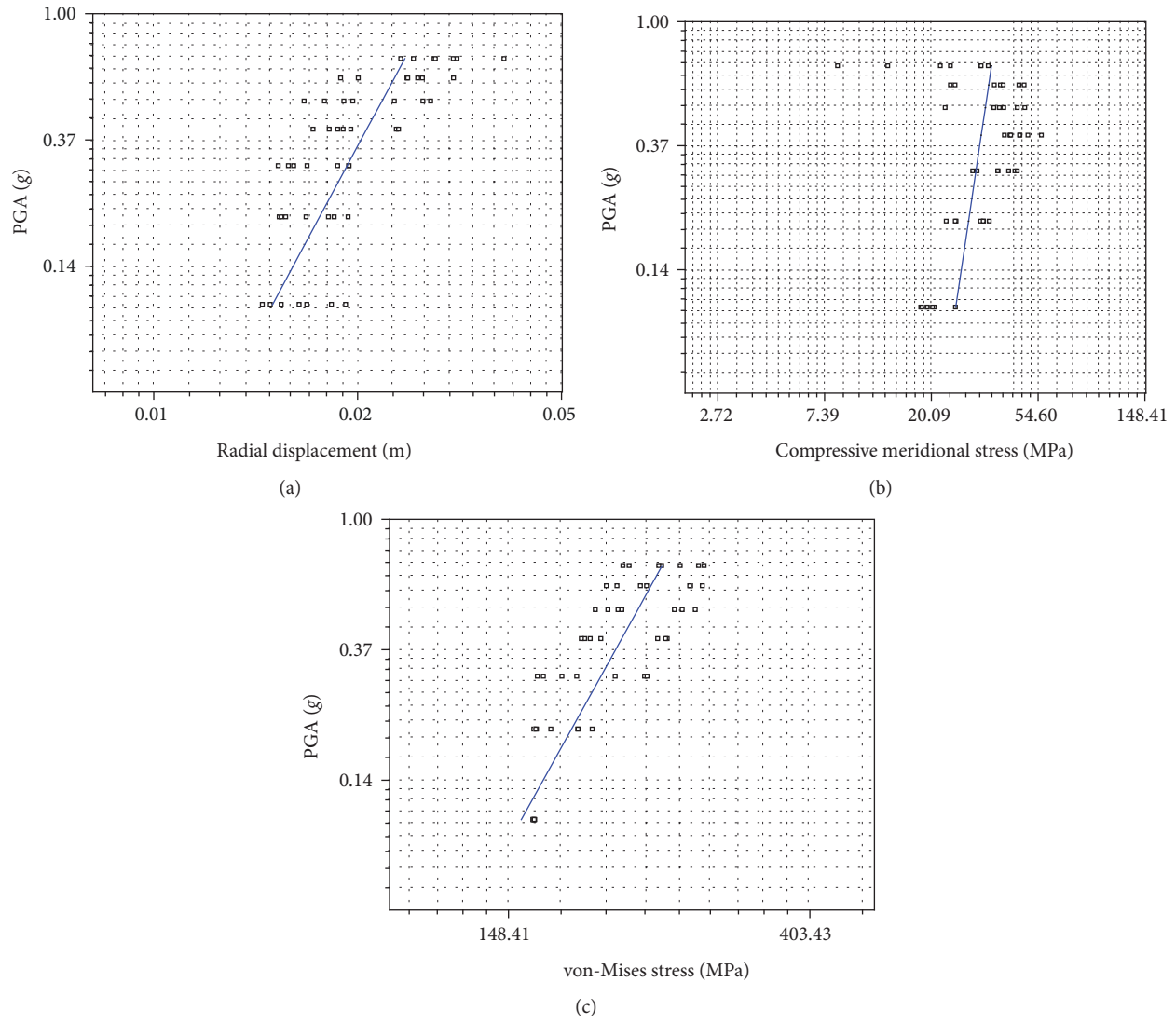

Figure 7: PSDMs of the unstiffened model for (a) elastic buckling, (b) elephant's foot buckling, and (c) steel yielding.

The impacts of the ring stiffeners and hydrodynamic forces owing to the oscillating liquid are investigated through nonlinear time-history analyses by employing an input ground motion of M_L4.0 and 0.4 g. Figure 8 depicts the deformed shapes of the unstiffened and ring-stiffened models using the same deformation scale factor in ABAQUS. As shown in the figure, the deformation of the unstiffened model is observed to be much larger than that of the ring-stiffened model. More detailed results are quantitatively discussed with the radial displacement of the tank wall in the following section.

Figure 9 compares the von-Mises stress results of nonoscillating and oscillating liquid storage tanks without stiffeners. The objective of the comparative analysis is to understand the hydrodynamic effect. It is found in the figure that the oscillating liquid storage tank has a relatively higher level of stress compared to the nonoscillating tank, particularly at the lower part of the tank in which the maximum stress occurred. This phenomenon is due to the hydrodynamic forces of the impulsive component of the liquid. Hence, the steel yielding of the tank wall and the buckling phenomena are investigated in this study.

Figure 10 shows the stress distributions of the unstiffened and ring-stiffened tank models; the maximum von-Mises stress occurs at the lower part of the tank wall. It is also found that ring stiffeners have little contribution to reducing the stress, unlike deformation.

4.2. Seismic Fragility Curves. This study investigates the seismic fragility of liquid storage tanks for three limit states: elastic buckling, elephant's foot buckling, and steel yielding. The threshold value for elastic buckling is computed based on previous literature [50]. According to the Korea Meteorological Administration archives [10], the earthquake on September 12, 2016 was the largest earthquake event and the PGA was approximately 0.43g PGA. In addition, the Next Generation Attenuation Relationships for Western US (NGA-West2) ground motion prediction equations (GMPEs) [51]

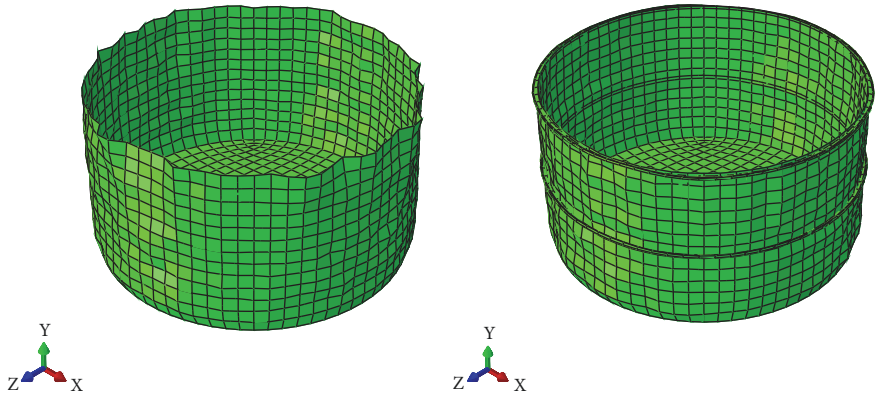

(a) (b)

Figure 8: Deformed shapes of liquid storage tanks (M_L4.0, 0.4 g PGA) for the (a) unstiffened and (b) ring-stiffened models.

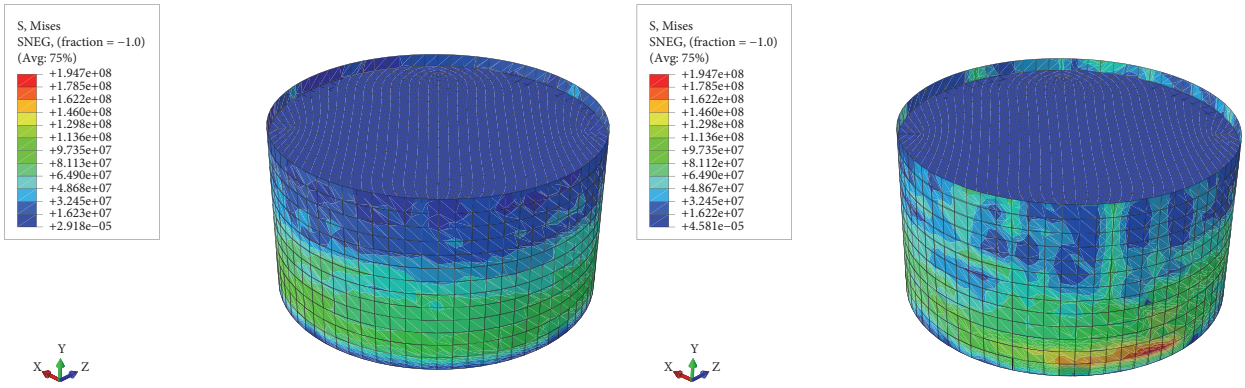

(a) (b)

Figure 9: Hydrodynamic effect of the liquid storage tank (M_L4.0, 0.4 g PGA) with: (a) non-oscillating, and (b) oscillating liquids.

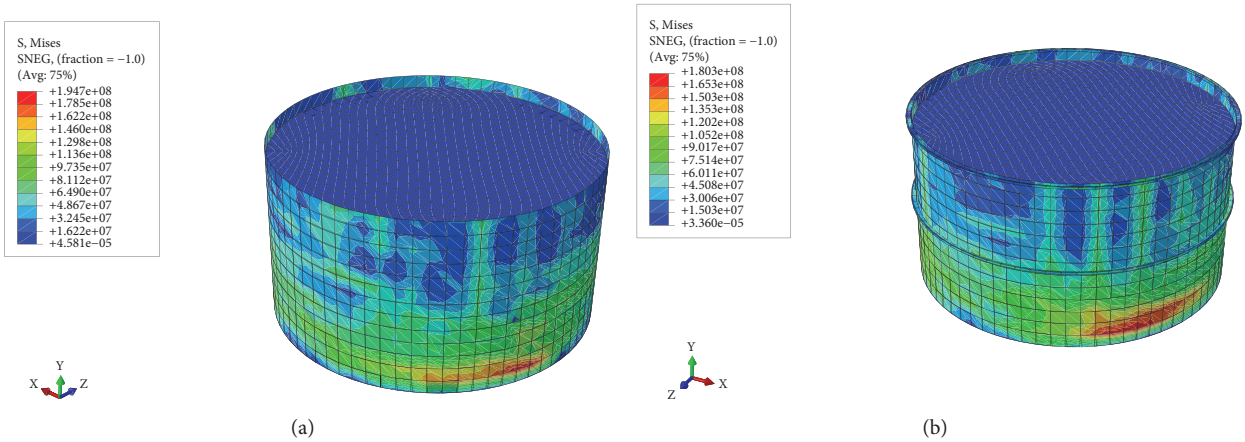

(a) (b)

Figure 10: Structural responses in terms of von-Mises stress (M_L4.0, 0.4 g PGA) of the: (a) unstiffened and (b) ring-stiffened models.

yields median PGAs + one standard deviation up to 0.7g for a M_L5.4 earthquake when a source-to-site distance is 2 km (which is a feasible scenario for Korea). Based on these, the radial displacement is investigated up to 0.7g PGA in this numerical example.

In addition, the Budiansky-Roth criterion is widely used to obtain the dynamic buckling load for a tank [9, 13, 14]. The critical point at which the radial displacement suddenly increases as the earthquake intensity increases is regarded as the dynamic buckling load, which is identified by the

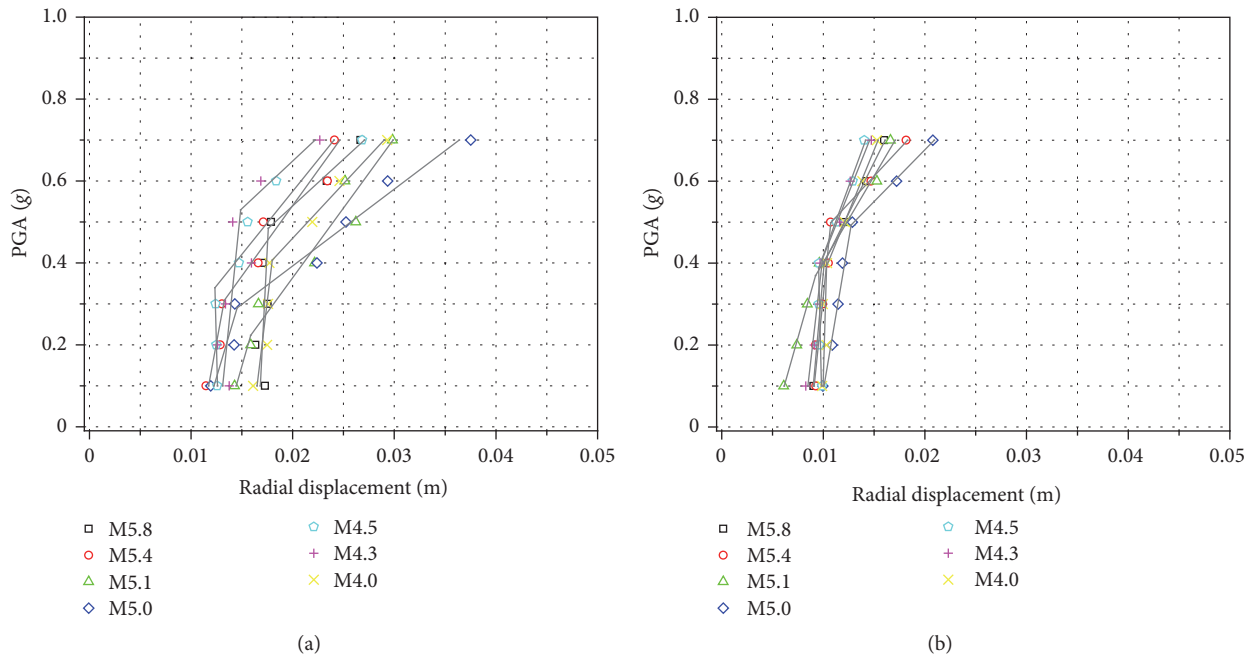

Figure 11: Pseudo-equilibrium paths: (a) unstiffened and (b) ring-stiffened models.

Table 5: Statistical parameters of the capacity and demand.

Model type	Limit state	Sc	β_C	$\beta_{D\|IM}$
Unstiffened tank	Elastic buckling	0.0151 (m)	0.1368	0.2011
	Elephant's foot buckling	36.5227 (MPa)	0.0970	0.3672
	Steel yielding	247.6041 (MPa)	0.0699	0.1128
Ring-stiffened tank	Elastic buckling	0.0103 (m)	0.1102	0.1550
	Elephant's foot buckling	31.3111 (MPa)	0.2192	0.4450
	Steel yielding	247.6041 (MPa)	0.0699	0.1157

pseudo-equilibrium path relating the *IM* (i.e., PGA in this study) and maximum radial displacement, as shown in Figure 11. The nodes on the upper part of the tank are monitored in this study, which is related to elastic buckling, and the critical points are estimated from the pseudo-equilibrium paths to be 0.0152 m and 0.0104 m for unstiffened and ring-stiffened tanks, respectively.

To determine the threshold value for elephant's foot buckling, the buckling stress capacity (σ_{cap}) and compressive meridional stress demand (σ_{dem}) are analyzed and plotted in the PGA-stress plane, and then the intersection point is estimated [40]. The compressive meridional stress demand is analyzed from a nonlinear time-history analysis. The buckling stress capacity is computed using the empirical equation [52], which is also adopted in Eurocodes 8-4 [53]:

$$\sigma_{cap} = \sigma_{c1}\left[1 - \frac{pR_t}{t_w f_y}\right]\left(1 - \frac{1}{1.12 + r^{1.15}}\right)\left[\frac{r + f_y/250}{r+1}\right] \quad (6)$$

where σ_{c1} ($=0.6Et_w/R_t$) is the ideal critical buckling stress, E the steel elastic modulus, t_w the wall thickness, and R_t the tank radius. r is equal to $(R_t/t_w)/400$ and f_y is the steel yield strength. p is the maximum interior pressure, which is the sum of the hydrostatic pressure and hydrodynamic pressure of impulsive component (p_i). The latter pressure is estimated by

$$p_i(\xi, \zeta, \theta, t) = C_i(\xi, \zeta)\,\rho H \cos(\theta)\, A_g(t) \quad (7)$$

where ξ, ζ, and θ are the nondimensional coordinates of radius, height, and angle, respectively. $C_i(\xi, \zeta)$ indicates the distribution of p_i in the vertical direction, ρ is the liquid density, and H is the liquid height in the tank. $A_g(t)$ is the ground acceleration time-history.

Failure probabilities are calculated by the standard normal cumulative distribution function using (5). Table 5 presents the statistical parameters of the capacity and demand: S_C, β_C, and $\beta_{D|IM}$. The median value of S_D is estimated by the PSDM. The value of β_C for steel yielding is obtained by referring to the probabilistic model code from the Joint Committee on Structural Safety [54].

From the PSDMs and statistical parameters, seismic fragility curves are derived with the given limit states (Figure 12). As shown in the fragility curves, the steel tank is more vulnerable to elastic buckling than elephant's foot

Table 6: Failure probabilities to elastic buckling.

PGA (g)	0.1	0.12	0.14	0.16	0.18	0.20	0.22	0.24
Unstiffened tank	0.178	0.251	0.323	0.391	0.454	0.512	0.563	0.610
Ring-stiffened tank	0.079	0.129	0.186	0.246	0.307	0.366	0.423	0.476
Difference	0.099	0.122	0.137	0.145	0.147	0.146	0.140	0.134
PGA (g)	0.26	0.28	0.30	0.32	0.34	0.36	0.38	0.40
Unstiffened tank	0.651	0.688	0.721	0.750	0.775	0.798	0.818	0.836
Ring-stiffened tank	0.526	0.571	0.612	0.650	0.684	0.715	0.743	0.767
Difference	0.125	0.117	0.109	0.100	0.091	0.083	0.075	0.069

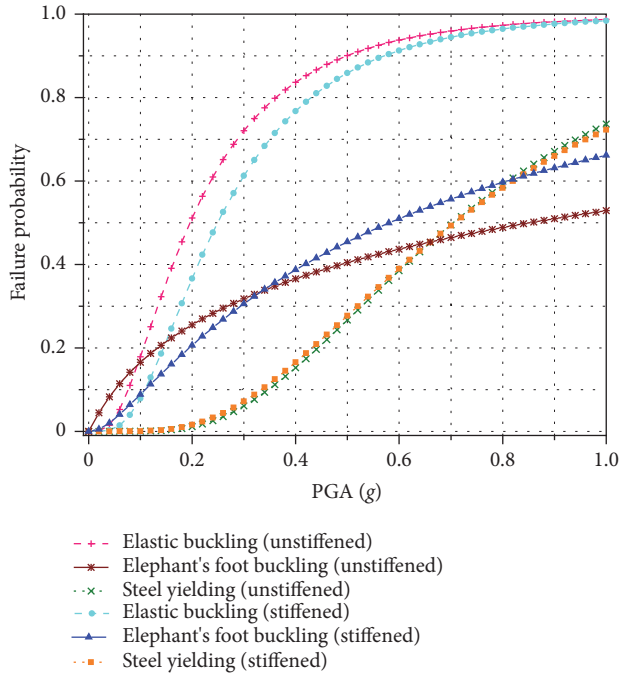

Figure 12: Seismic fragility curves.

buckling and steel yielding; the maximum differences in the failure probabilities of elastic buckling and steel yielding and of elastic buckling and steel yielding are 0.501 at 0.58 g PGA and 0.687 at 0.38 g PGA for the unstiffened model, respectively. This means that a large deflection of the upper part of the tank wall, due to the elastic buckling instability, is likely to occur prior to reaching the elephant's foot buckling capacity and yield strength of the steel.

When comparing the failure probabilities of the ring-stiffened and unstiffened models at the same earthquake intensities in terms of elastic buckling, although the ring stiffener has little influence on the seismic fragility to steel yielding, it can reduce the failure probability owing to elastic buckling. To investigate this further, the failure probabilities between 0.1 and 0.4 g, which is the range corresponding to past major earthquakes in southeast Korea, are provided in Table 6.

The table shows that the ring-stiffener reduces the failure probability of the steel tank to elastic buckling by 0.069–0.147. In particular, the maximum difference is 0.147 at 0.18 g PGA. From these results, it is confirmed that a ring-stiffener can significantly reduce the seismic failure risk of liquid-containing steel tanks. In contrast, in the case of elephant's foot buckling, the ring stiffeners have no practical effect, especially for PGA levels larger than 0.34 g PGA.

5. Conclusions

This study analytically derives seismic fragility curves of anchored liquid storage tanks. Because the characteristics of earthquake ground motions are important for influencing the seismic vulnerability of structures, real earthquake ground motions recorded in Ulsan Seismological Observatory are used in nonlinear time-history analyses. All components of the ground motions are included in high a/v levels representing high-frequency ground motions, short durations, and small-to-medium magnitude earthquakes.

Hydrodynamic forces owing to an oscillating liquid in a tank are also a significant cause of structural damage to liquid storage tanks. Thus, this study develops two advanced FE models with and without ring stiffeners to consider hydrodynamic effect and analyze yielding stress acted on the tank walls. Furthermore, since the buckling phenomenon mainly occurs in thin-walled structures such as steel liquid storage tanks, the elastic buckling and elephant's foot buckling phenomena are also investigated.

Seismic fragility curves with different limit states (i.e., elastic buckling, elephant's foot buckling, and steel yielding) were successfully derived based on PSDMs. By using fragility curves, it is observed that the steel liquid storage tank is more vulnerable to elastic buckling than elephant's foot buckling and steel yielding with maximum differences of failure probabilities (0.501 at 0.58 g PGA and 0.687 at 0.38 g PGA) for the unstiffened model. Furthermore, although there was little effect of the ring stiffener on reducing the steel yielding fragility, it is observed that the failure probabilities of the ring-stiffened tank to elastic buckling decreases up to 0.147 compared with the unstiffened one, which indicates that a ring-stiffener can significantly reduce the seismic failure risk of liquid-containing steel tanks. In contrast to the case of elastic buckling, the ring stiffeners had no practical effect on elephant's foot buckling fragility since the failure probabilities of the ring-stiffened model were larger than those of the unstiffened model for PGA levels larger than 0.34 g PGA.

Appendix

Table 7 summarizes the occurrence of earthquake events in the southeastern Korean Peninsula. These records

Table 7: Earthquake records occurred in the Southeastern Korean Peninsula [19].

Record No.	M_L	Date & Time	Epicenter	
			Latitude (°)	Longitude (°)
1	3.5	12/25/2017 16:19	36.11	129.36
2	3.6	11/20/2017 06:05	36.14	129.36
3	3.5	11/19/2017 23:45	36.12	129.36
4*	4.3	11/15/2017 16:49	36.12	129.36
5	3.5	11/15/2017 15:09	36.09	129.34
6	3.6	11/15/2017 14:32	36.10	129.36
7*	5.4	11/15/2017 14:29	36.12	129.36
8	3.1	04/15/2017 11:31	36.11	129.36
9	3.3	03/31/2017 13:46	35.78	129.20
10	3.3	01/06/2017 05:31	35.75	129.17
11	3.3	12/14/2016 17:20	35.76	129.17
12	3.3	12/12/2016 17:53	35.76	129.18
13	3.3	10/10/2016 22:59	35.75	129.18
14	3.0	10/02/2016 20:53	35.75	129.19
15	3.1	09/28/2016 16:34	35.76	129.18
16	3.5	09/21/2016 11:53	35.75	129.18
17*	4.5	09/19/2016 20:33	35.74	129.18
18	3.0	09/14/2016 00:48	35.75	129.18
19	3.0	09/13/2016 14:31	35.76	129.18
20	3.2	09/13/2016 08:24	35.76	129.17
21	3.1	09/13/2016 00:37	35.78	129.21
22	3.1	09/12/2016 23:52	35.75	129.18
23	3.0	09/12/2016 20:38	35.78	129.20
24	3.6	09/12/2016 20:34	35.78	129.19
25*	5.8	09/12/2016 20:32	35.76	129.19
26	3.1	09/12/2016 20:10	35.77	129.18
27	3.1	09/12/2016 19:48	35.77	129.19
28*	5.1	09/12/2016 19:44	35.77	129.19
29*	5.0	07/05/2016 20:33	35.51	129.99
30	3.0	06/03/2016 04:53	36.39	127.92
31	3.0	01/06/2016 20:39	36.01	128.07
32	3.2	11/24/2015 11:27	35.67	129.82
33	3.8	09/25/2014 02:26	35.07	129.94
34	3.5	09/23/2014 15:27	35.80	129.41
35	3.5	07/03/2014 21:57	35.66	129.76
36	3.0	03/28/2014 10:40	36.47	127.93
37	3.6	10/11/2013 16:06	36.46	129.61
38	3.0	08/13/2013 00:36	36.91	129.44
39	3.1	08/12/2013 04:33	35.66	129.75
40	3.5	02/05/2013 21:25	35.77	127.97
41	3.1	02/04/2013 05:39	36.55	128.90
42	3.0	11/22/2012 03:04	35.22	127.97
43	3.4	05/30/2012 02:48	36.57	129.57
44	3.2	02/24/2012 09:05	35.20	129.93
45	3.0	11/02/2011 07:20	35.54	130.65
46	3.2	05/29/2011 10:22	35.58	128.75
47	3.2	03/28/2011 13:50	35.97	129.95
48	3.3	02/16/2010 18:53	35.63	129.95
49	3.0	06/28/2009 22:07	35.78	128.29
50*	4.0	05/02/2009 07:58	36.56	128.71
51	3.0	01/13/2009 19:07	36.47	129.64
52	3.5	12/19/2008 17:53	36.49	129.68

*Selected input ground motions for nonlinear time-history analyses.

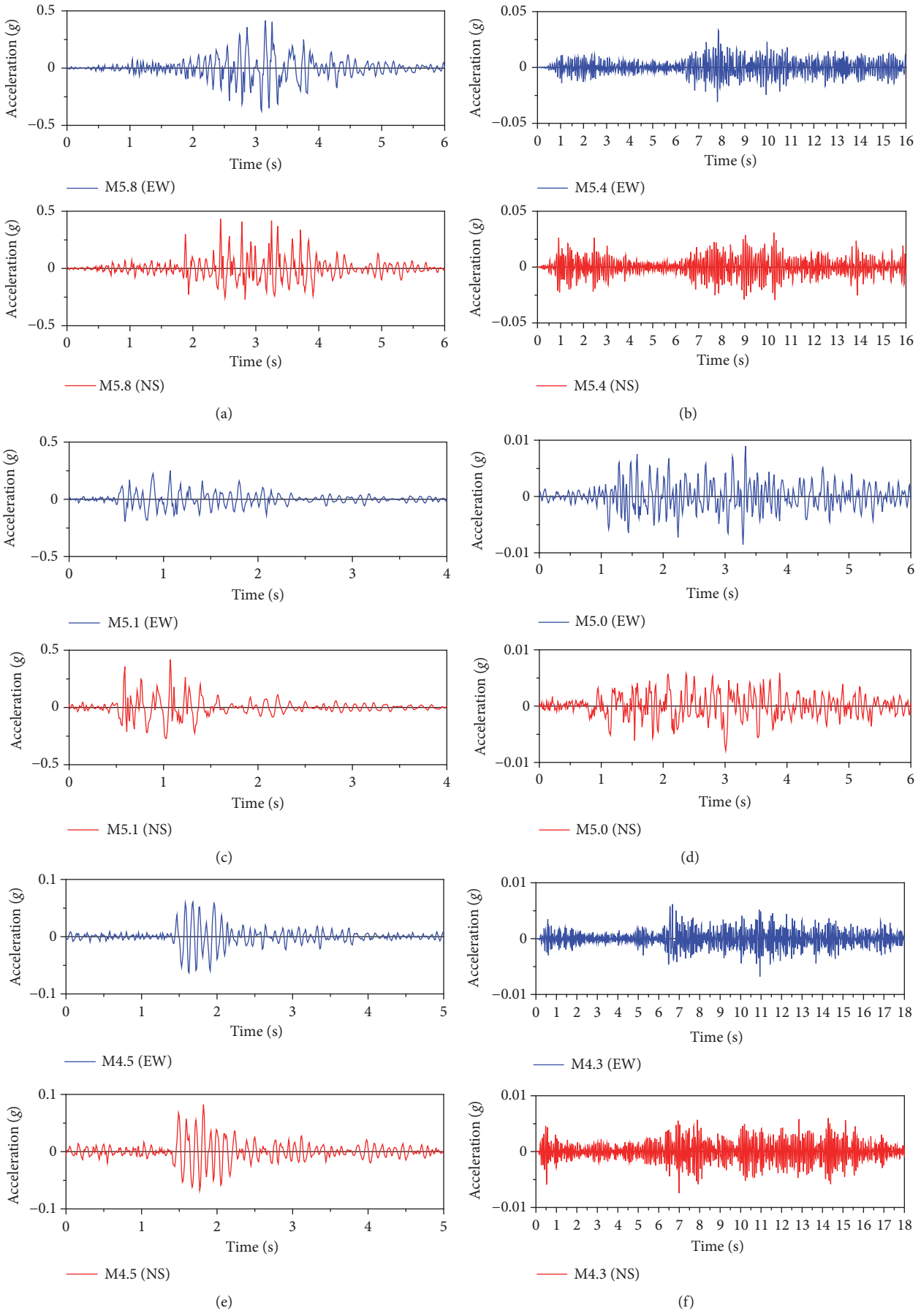

Figure 13: Continued.

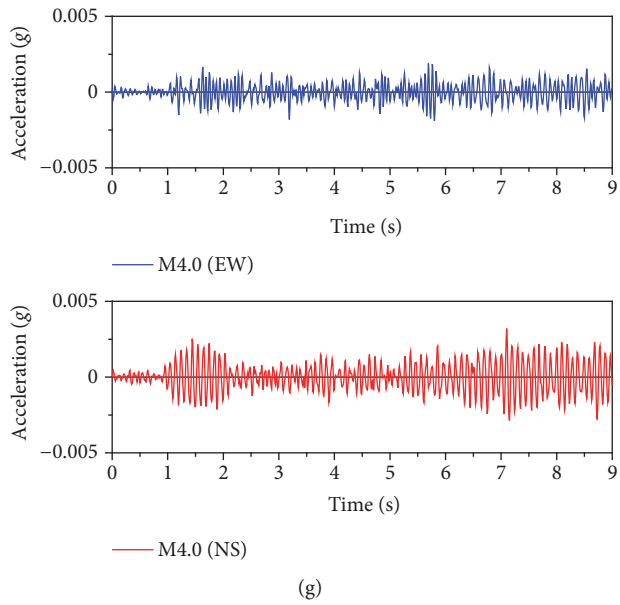

FIGURE 13: Input ground motions used in the nonlinear time-history analyses: (a) M_L5.8, (b) M_L5.4, (c) M_L5.1, (d) M_L5.0, (e) M_L4.5, (f) M_L4.3, and (g) M_L4.0.

correspond to earthquake events of $M_L \geq 3.0$ in the last 10 years. There were 52 earthquake events observed at the Ulsan Seismological Observatory. The records were collected from the NECIS database. Figure 13 shows the selected input ground motions used in the time-history analyses.

Data Availability

The data used to support the findings of this study are available from the corresponding author upon request.

Conflicts of Interest

The authors declare that there are no conflicts of interest regarding the publication of this paper.

Acknowledgments

This work was supported by the 2019 Research Fund (1.190047.01) of UNIST (Ulsan National Institute of Science and Technology). This research was also supported by a grant (19SCIP-B146959-02) from Construction technology research program funded by Ministry of Land, Infrastructure and Transport of Korean government.

References

[1] H. Persson and A. Lönnermark, "Tank fires," Tech. Rep. SP Report 2004:14, SP Swedish National Testing and Research Institute, Boras, Sweden, 2004.

[2] "Korea Industrial Complex Corporation," 2018. http://www.kicox.or.kr/.

[3] O. Kwon and A. Elnashai, "The effect of material and ground motion uncertainty on the seismic vulnerability curves of RC structure," *Engineering Structures*, vol. 28, no. 2, pp. 289–303, 2006.

[4] D. Moon, Y. Lee, and S. Lee, "Fragility analysis of space reinforced concrete frame structures with structural irregularity in plan," *Journal of Structural Engineering*, vol. 144, no. 8, Article ID 04018096, 2018.

[5] Y. Lee and D. Moon, "A new methodology of the development of seismic fragility curves," *Smart Structures and Systems*, vol. 14, no. 5, pp. 847–867, 2014.

[6] S. Lee, Y.-J. Lee, and H.-Y. Tak, "Fragility assessment of liquid storage tanks under seismic loads by integration of two software packages," in *Proceedings of the 12th International Conference on Structural Safety and Reliability (ICOSSAR2017)*, TU Wien, Vienna, Austria, August 2014.

[7] X. Chu, J. M. Ricles, and S. N. Pakzad, "Seismic fragility analysis of the smithsonian institute museum support center," *Earthquake Spectra*, vol. 33, no. 1, pp. 85–108, 2017.

[8] Y. Pang, X. Wu, G. Shen, and W. Yuan, "Seismic fragility analysis of cable-stayed bridges considering different sources of uncertainties," *Journal of Bridge Engineering*, vol. 19, no. 4, Article ID 04013015, 2013.

[9] N. Buratti and M. Tavano, "Dynamic buckling and seismic fragility of anchored steel tanks by the added mass method," *Earthquake Engineering & Structural Dynamics*, vol. 43, no. 1, pp. 1–21, 2014.

[10] H. N. Phan, F. Paolacci, and S. Alessandri, "Fragility analysis methods for steel storage tanks in seismic prone areas," in *Proceedings of the ASME 2016 Pressure Vessels and Piping Conference*, American Society of Mechanical Engineers, British Columbia, Canada, July 2016.

[11] G. W. Housner, "The dynamic behavior of water tanks," *Bulletin of Seismological Society of America*, vol. 53, no. 2, pp. 381–387, 1963.

[12] A. S. Veletsos, "Seismic effects in flexible liquid storage tanks," in *Proceedings of the 5th world conference on earthquake engineering*, pp. 630–639, Roma, Italy, June 1974.

[13] J. Virella, L. Godoy, and L. Suárez, "Dynamic buckling of anchored steel tanks subjected to horizontal earthquake excitation," *Journal of Constructional Steel Research*, vol. 62, no. 6, pp. 521–531, 2006.

[14] M. Djermane, D. Zaoui, B. Labbaci, and F. Hammadi, "Dynamic buckling of steel tanks under seismic excitation: numerical evaluation of code provisions," *Engineering Structures*, vol. 70, pp. 181–196, 2014.

[15] M. Sobhan, F. Rofooei, and N. K. Attari, "Buckling behavior of the anchored steel tanks under horizontal and vertical ground motions using static pushover and incremental dynamic analyses," *Thin-Walled Structures*, vol. 112, pp. 173–183, 2017.

[16] F. Paolacci, H. N. Phan, D. Corritore, S. Alessandri, O. S. Bursi, and M. S. Reza, "Seismic fragility analysis of steel storage tanks," in *Proceedings of the 5th ECCOMAS Thematic Conference on Computational Methods in Structural Dynamics and Earthquake Engineering, COMPDYN 2015*, pp. 2054–2065, Crete, Greece, May 2015.

[17] A. Di Carluccio, G. Fabbrocino, and G. Manfredi, "FEM seismic analysis of steel tanks for oil storage in industrial facilities," in *Proceedings of the 14th World Conference on Earthquake Engineering*, Beijing, China, October 2008.

[18] P. F. Adams, "High-strength steels for plastic design," *Engineering Journal, AISC*, vol. 3, no. 4, p. 150, 1966.

[19] "National Earthquake Comprehensive Information System," 2017. http://necis.kma.go.kr/.

[20] T. G. Cork, J. H. Kim, G. P. Mavroeidis, J. K. Kim, B. Halldorsson, and A. S. Papageorgiou, "Effects of tectonic regime and soil conditions on the pulse period of near-fault ground motions," *Soil Dynamics and Earthquake Engineering*, vol. 80, pp. 102–118, 2016.

[21] C. S. Kim, "Overview of the techonic environment in Korea with reference to HLW disposal," Tech. Rep. KR9700364, Korea Atomic Energy Research Institute, Daejeon, South Korea, 1997.

[22] H. Jung, Y. Jang, and B. G. Jo, "Upper-crust shear-wave velocity of South Korea constrained by explosion and earthquake data," *Bulletin of the Seismological Society of America*, vol. 101, no. 6, pp. 2819–2832, 2011.

[23] T. J. Zhu, A. C. Heidebrecht, and W. K. Tso, "Effect of peak ground acceleration to velocity ratio on ductility demand of inelastic systems," *Earthquake Engineering & Structural Dynamics*, vol. 16, no. 1, pp. 63–79, 1988.

[24] W. Tso, T. Zhu, and A. Heidebrecht, "Engineering implication of ground motion A/V ratio," *Soil Dynamics and Earthquake Engineering*, vol. 11, no. 3, pp. 133–144, 1992.

[25] T. Sawada, K. Hirao, H. Yamamoto, and O. Tsujihara, "Relation between maximum amplitude ratio (a/v, ad/v2) and spectral parameters of earthquake ground motion," in *Proceedings of the Tenth World Conference on Earthquake Engineering*, pp. 617–622, Madrid, Spain, July 1992.

[26] D. H. Sheen, I. S. Lim, J. H. Park, and H. C. Chi, "Earthquake magnitude determination using P phase for earthquake early warning," *Journal of the Geological Society of Korea*, vol. 48, no. 1, pp. 101–111, 2012 (Korean).

[27] H. Kanamori, P. Maechling, and E. Hauksson, "Continuous monitoring of ground-motion parameters," *Bulletin of the Seismological Society of America*, vol. 89, no. 1, pp. 311–316, 1999.

[28] National Research Council Canada (NRCC), *National Building Code of Canada*, Ottawa, ON, Canada, 1985.

[29] M. Paz, *International Handbook of Earthquake Engineering: Codes, Programs, and Examples*, Chapman & Hall, New York, NY, USA, 1994.

[30] American Society of Civil Engineers (ASCE), *ASCE/SEI 7-05 Minimum Design Loads for Buildings and Other Structures*, Reston, VA, USA, 2005.

[31] European Committee for Standardization (CEN), *Eurocode 8: Design of Structures for Earthquake Resistance - Part 1: General Rules, Seismic Actions and Rules for Buildings*, Brussels, Belgium, 2004.

[32] Building Seismic Safety Council (BSSC), *NEHRP Recommended Provisions for Seismic Regulations for New Buildings and Other Structures, Part 1: Provisions (FEMA 368)*, Washington, DC, USA, 2000.

[33] K. Beyer and J. J. Bommer, "Selection and scaling of real accelerograms for bi-directional loading: a review of current practice and code provisions," *Journal of Earthquake Engineering*, vol. 11, no. 1, pp. 13–45, 2007.

[34] European Strong-Motion Database. 2017. http://isesd.hi.is/.

[35] H. N. Phan, F. Paolacci, and S. Alessandri, "Enhanced seismic fragility analysis of unanchored steel storage tanks accounting for uncertain modeling parameters," *Journal of Pressure Vessel and Technology*, vol. 141, no. 1, Article ID 010903, 2019.

[36] H. N. Phan, F. Paolacci, and P. Mongabure, "Nonlinear finite element analysis of unanchored steel liquid storage tanks subjected to seismic loadings," in *Proceedings of the ASME PVP (American Society of Mechanical Engineers, Pressure Vessels and Piping Division) 2017 Conference*, vol. 8, Hawaii, HI, USA, 2017.

[37] American Petroleum Institute (API), *API Standard 650 - Welded Tanks for Oil Storage*, Washington, DC, USA, 2013.

[38] T. Sun, E. Azzuni, and S. Guzey, "Stability of open-topped storage tanks with top stiffener and one intermediate stiffener subject to wind loading," *Journal of Pressure Vessel Technology*, vol. 140, no. 1, Article ID 011204, 2018.

[39] J. E. Padgett and R. DesRoches, "Methodology for the development of analytical fragility curves for retrofitted bridges," *Earthquake Engineering & Structural Dynamics*, vol. 37, no. 8, pp. 1157–1174, 2008.

[40] K. Bakalis, D. Vamvatsikos, and M. Fragiadakis, "Seismic risk assessment of liquid storage tanks via a nonlinear surrogate model," *Earthquake Engineering & Structural Dynamics*, vol. 46, no. 15, pp. 2851–2868, 2017.

[41] K. R. Mackie and B. Stojadinović, "Comparison of incremental dynamic, cloud, and stripe methods for computing probabilistic seismic demand models," in *Proceedings of the Structures Congress 2005: Metropolis and Beyond*, pp. 1–11, New York, NY, USA, April 2005.

[42] B. G. Nielson and R. DesRoches, "Analytical seismic fragility curves for typical bridges in the central and southeastern United States," *Earthquake Spectra*, vol. 23, no. 3, pp. 615–633, 2007.

[43] S. Mangalathu, E. Choi, H. C. Park, and J.-S. Jeon, "Probabilistic seismic vulnerability assessment of tall horizontally curved concrete bridges in California," *Journal of Performance of Constructed Facilities*, vol. 32, no. 6, Article ID 04018080, 2018.

[44] J.-S. Jeon, J.-H. Park, and R. Desroches, "Seismic fragility of lightly reinforced concrete frames with masonry infills," *Earthquake Engineering & Structural Dynamics*, vol. 44, no. 11, pp. 1783–1803, 2015.

[45] J. Jeon, R. DesRoches, T. Kim, and E. Choi, "Geometric parameters affecting seismic fragilities of curved multi-frame concrete box-girder bridges with integral abutments," *Engineering Structures*, vol. 122, pp. 121–143, 2016.

[46] S. Mangalathu, J.-S. Jeon, J. E. Padgett, and R. DesRoches, "Performance-based grouping methods of bridge classes for

regional seismic risk assessment: Application of ANOVA, ANCOVA, and non-parametric approaches," *Earthquake Engineering & Structural Dynamics*, vol. 46, no. 14, pp. 2587–2602, 2017.

[47] C. A. Cornell, F. Jalayer, R. O. Hamburger, and D. A. Foutch, "Probabilistic basis for 2000 SAC federal emergency management agency steel moment frame guidelines," *Journal of Structural Engineering*, vol. 128, no. 4, pp. 526–533, 2002.

[48] D. Vamvatsikos and C. Allin Cornell, "Incremental dynamic analysis," *Earthquake Engineering & Structural Dynamics*, vol. 31, no. 3, pp. 491–514, 2002.

[49] R. P. Dhakal, J. B. Mander, and N. Mashiko, "Identification of critical ground motions for seismic performance assessment of structures," *Earthquake Engineering & Structural Dynamics*, vol. 35, no. 8, pp. 989–1008, 2006.

[50] B. Budiansky and R. S. Roth, "Axisymmetric dynamic buckling of clamped shallow spherical shells," in *Collected Papers on Instability of Shell Structures*, pp. 597–606, NASA-TN-1510, USA, 1962.

[51] Y. Bozorgnia, N. A. Abrahamson, L. A. Atik et al., "NGA-West2 research project," *Earthquake Spectra*, vol. 30, no. 3, pp. 973–987, 2014.

[52] J. M. Rotter, "Local collapse of axially compressed pressurized thin steel cylinders," *Journal of Structural Engineering*, vol. 116, no. 7, pp. 1955–1970, 1990.

[53] European Committee for Standardization (CEN), *Eurocode 8: Design of Structures for Earthquake Resistance - Part 4: Silos, Tanks And Pipelines*, Brussels, Belgium, 2006.

[54] Joint Committee on Structural Safety. 2017. http://www.jcss.byg.dtu.dk/.